Journal of Biomimetics, Biomaterials and Biomedical Engineering Vol. 20 (2014) pp 73-85
Online available since 2014/Jun/06 at www.scientific.net

doi:10.4028/www.scientific.net/JBBBE.20.73

Bone Tissue Response in a Metallic Bone Architecture Microstructure

Tamiye Simone Goia[1, a], Kalan Bastos Violin[1,b], Carola Gomez Ágreda[1,c], José Carlos Bressiani[1,d] and Ana Helena de Almeida Bressiani[1,e]

[1]Av. Professor Lineu Prestes, 2242, Instituto de Pesquisas Energéticas e Nucleares, São Paulo, SP, Brazil

[a]tsgoia@ipen.br, [b]kbviolin@ipen.br, [c]cgagreda@ipen.br, [d]jcbressia@ipen.br, [e]abressia@ipen.br

Keywords: Porosity, Titanium, Bone Microstructure, Natural Polymers

Abstract. Porous metallic structures have been developed to mimic the natural bone architecture, having interconnected porosity, disposing enough room to cell migration, anchoring, vascularization, nourishing and proliferation of new bone tissue. Research involving porous titanium has been done with purpose to achieve desirable porosity and increasing of bone-implant bond strength interface. Samples of titanium were prepared by powder metallurgy (PM) with addition of different natural polymers (cornstarch, rice starch, potato starch and gelatin) at proportion of 16wt%. In aqueous solution the hydrogenated metallic powder (TiH_2) and the polymer were mixed, homogenized and frozen in molds near net shape. The water was removed in kiln and the polymer by thermal treatment in air- (350ºC/1h) before sintering in high-vacuum (1300ºC/1h). The biological evaluation was performed by *in vivo* test in rabbits. Histological analysis was performed by scanning electron microscopy (SEM), energy dispersive spectroscopy (SEM-EDS) and fluorescence microscopy (FM). The processing methodologies using natural low cost additives propitiate the production of porous metallic implants in a simplified manner, with different porosities, proper porosity degree (40%), distribution, and maximum pore size of 80 µm to 220 µm depending of natural polymer used. The samples added with rice starch, presented the most similar structure organization when compared to the bone tissue microstructure organization of the trabecular bone. All implants osseointegrated, the pore microarchitecture and its interconnected network allowed bone ingrowth in all pore sizes, but the continuous bone maturation occurred in pores bigger than 80 µm.

Introduction

Metallic biomaterials are widely used in medicine, for replacing, supporting or repairing bone tissues that were lost or suffered injuries. The main fields of application, as orthopedics and dentistry, expect from materials some desirable properties of those particular metals like mechanical strength, corrosion resistance and non-toxicity among others. The major clinical application of metallic biomaterials is as endosseous implants, for that reason, many studies research the interaction between bone and the material [1, 2, 3]. The bone tissue is the main responsible for providing stability and support to the body, being a highly specialized support tissue. The bone is a highly hierarchical nanomaterial composite, a mineralized hard tissue able to modify its own structure to meet the physical and metabolic need in response to physiological and environmental factors. The complex network of cortical and trabecular bone cannot be reproduced by alloplastic materials yet, since not only the inorganic parts are involved in that interaction, but also the organic content which have an important role on the biofunctional property of bone [4]. Architecturally and functionally, cortical bone has considerable similarity to the metallic machined implant regularly used in conventional treatment. Nevertheless the developing of a trabecular metallic structure, which mimics the architectural appearance of trabecular bone, changes the perspective of metallic biomaterials requirements to be addressed during the rehabilitation process.

In the process of repair, the healing of bone-implant interface passes through the same steps as a direct bone fracture, following an orderly sequence of events. After primary stabilization and serum protein adsorption on the implant, the initial healing begins with the formation of coagulum between the bone and the implant, with subsequent clot organization allowing cells to adhere at the

implant surface and forming blood vessels. Osteoprogenitor cells proliferate and differentiate in this organized environment into osteoblasts, thus promoting the deposition of mineral content to form the bone tissue through the implant surface [5, 6].

The topography of the implant is one of the factors that influence the process of bone repair to osseointegrate the implant. Although implants machined have been used for many years, studies have shown that the increase in surface roughness tends to enhance, not only the surface area between the bone and the implant, but also the bond strength of the interface [7, 8]. Among the modifications to prevailing topography, porosity in implants is quite interesting because it allows the occurrence of the phenomenon of tissue invasion into the pores, known as bone ingrowth [9]. The porous implants must have interconnected porosity with spaces that allow the maintenance required for vascular continuous nourishing for mineralization of bone tissue. The success of remodeling process and consequently the success of the implantation are related to this characteristic. Thus, both the pore channels and the interconnection must have sufficient size to the infiltration of cells responsible for formation of the tissue matrix within the material, in order to meet the requirements for a desirable durable rehabilitation healing [10, 11, 12].

Titanium and its alloys are the main metal studied as porous implants by excellent mechanical properties and biological interactions. Research on porous titanium have been carried out in order to analyze issues related to the optimal size of pores, porosity and degree of their influence in increasing the bond strength of the bone-implant interface [13]. The pore size is a subject addressed by many authors due to its direct influence in the migration and maturation of osteoprogenitor cells. Some authors also determined that vascularization may not occur in pores of diameter with less than 100μm, and the reported optimal pore size fitted to proper bone and vascular reorganization, range between 100-500μm, although pore size around 10 to 20μm can allow bone growth, but without tissue penetration [9, 11, 14, 15, 16, 17].

One of the methods for production of trabecular metallic structures is based on powder metallurgy (PM). This technique allows the production of parts with complex shapes and dimensions close to the finals, near-net shape, avoiding the step of machining [13]. The manipulation of the metals in the form of particulate allows the addition of elements reaching a satisfactory structural homogeneity, and porosity [18, 19]. The production of porous structures has been proposed by various techniques, such as space-holder [18], metal injection mold (MIM) [20], freeze-cast [21], electron beam melting (EBM) [22] and prototyping [23].

Natural polymers such as starches are successfully used in the production of porous ceramic, and this technology can be transferred and adapted to process metals [24]. With sacrificial template techniques, such as suspension and space-holder, the starch is removed by thermal treatment, forming pores in the spaces once previously occupied by it, in the case of metals, oxidation during heat treatment may be a hindrance and can weaken the structure, thus to counteract these undesirable effects, hydrates can be used to mitigate this shortcoming. Regarding the technique of gel-casting, or suspension, the starch has the function of gelling agent by absorbing water and expanding volumetrically, actions relevant to the production of pores in the structure [24]. Other natural polymer that can be used as additive is gelatin, a collagen based substance, which has properties of biocompatibility, biodegradability and non-toxicity [19]. This study aims to apply the suspension technique for obtaining porous metallic implants using naturals polymers (cornstarch, rice starch, potato starch and gelatin) and evaluate these metallic trabecular structures *in vivo,* by the assessment of bone tissue response towards these implants with aid of electron and fluorescent microscopy.

Experimental Procedure

The processing of porous metallic implants using hydride titanium (TiH_2) powder and natural polymers (cornstarch, potato starch, rice starch and gelatin) followed the same procedures and protocols published previously at Goia, et al., 2013 and material physical characterizations of the porous metallic samples were evaluated and in accordance to the guidelines [25]. At this study, pore sizes and pore shapes of implants were characterized by scanning electron microscopy (SEM)

(Hitachi, Tabletop TM3000) and image analysis (ImagePro Plus 6.1 software). These results are related to the bone ingrowth process, on the *in vivo* study.

The technique to obtain porous structure involved pore formation by suspension technique, the metal powder was mixed in a suspension consisting of water and different natural polymers. The ratio used was 16% by weight of natural polymer from the total solids in hot water. Cylindrical molds were filled with the suspension aided by a syringe to remove bubbles. Immediately after filling the mold, it was frozen in liquid nitrogen and the sample removed and placed in freezer (-10°C). After 12 h, samples were placed in kiln (38°C) prior to thermal treatment (TT) and sintering. For the organic material decomposition and removal of carbon, all samples were TT in an oxidizing atmosphere at 350°C for 1 hour and heating rate of 1°C/min. The samples were sintered in a furnace of tungsten heating element with high vacuum (10^{-5} mBar) at 1300°C for 1 hour [25].

The near-net-shape process resulting porous implant size, was 3mm in diameter and 5mm in length, as a control was used a dense implant of cpTi machined with 2mm in diameter and 5mm in length. Before the *in vivo* test, all the implants were sterilized using 25kGy single dose of gamma radiation (Co^{60}, Gammacell model 220 of Nuclear and Energy Research Institute-IPEN).

For the mimicking study, trabecular structure of normal rabbit tibia bone was evaluated by SEM (Hitachi, Tabletop TM3000). The bone sample was put on series of sodium hypochlorite 0.5% during 7 days for removal of bone organic part, washed in water and dried at 38ºC.

For care and use of laboratory animals, the guidelines and regulations of Center of Biomedical Sciences (CB-IPEN) have been observed, and approved by the Animal Use Ethical Committee (CEUA-IPEN – Project nº 69/10). Five adult New Zealand White male rabbits weighting around 2.5 kg were anesthetized by an intramuscular injection of Ketamine (50mg/kg) + Xylazine (5mg/kg). Through an anteromedial approach into the proximal third of the tibia, 3 cortical bone defects were drilled in the left and right hind leg, 2 mm diameter for the control implant and 3mm diameter for the porous implants. After placing the implants, periosteum and skin were carefully closed with simple uninterrupted sutures. After the surgical procedure the rabbits received a intramuscular single dose of broad spectrum antibiotic (1mL per rabbit, Veterinary pentabiotic®, Forth Doge) and once a day dose, for three consecutive days, of analgesic agent (Tramadol hydrochloride, Pfizer, 3mg/kg) and anti-inflammatory agent (Ketoprofen, Sanofi-Aventis, 3mg/kg).

For the implant osseointegration, the animal experiment lasted 7 weeks to evaluate the bone ingrowth throughout the implant porosity. Aiming to follow up the bone formation through the experiment weeks, fluorescent bone markers with affinity for apatite were used. Each marker was administered via subcutaneous, once a week, for two consecutive weeks in the following order and respective dose per application: Tetracyclin (60mg/kg), Alizarin (30mg/kg) and Calcein (10mg/kg). The rabbits were euthanized following the procedure of general anesthesia until loss of reflexes (Ketamine 50mg/kg in association with Xylazine 10mg/kg), intravenous injection of potassium chloride (35 mg/kg) to stop the heart and subsequently all vital signs. The soft tissues were dissected and the compound of bone-implant was sampled using a diamond cutting disk. The samples were kept in formalin 10% solution for 30 days. The procedure of embedding the samples in resin followed the manufacturer's protocol of the methyl methacrylate resin Technovit® 9100 NEU. The blocks were cut using Isomet® and the slices polished to obtain the histological slides of undecalcified bone-implant. The histological slides were submitted to light microscopy using fluorescent microscopic analysis (FM analysis) (Leica Microsystems, Leica DM2500/DFC310FX) and scanning electron microscopy - energy dispersive spectroscopy analysis (SEM-EDS analysis) (Hitachi, Tabletop TM3000).

The FM analysis and SEM-EDS analysis were both performed using the polished histological slides of undecalcified bone-implant without staining. For the FM analysis each image was obtained in greyscale monochromatic with three different filters: D, N2.1 and I3 (Leica Microsystems), respectively for each bone marker used, Tetracycline, Alizarin and Calcein. The merging and tinting of images was performed using ImagePro Plus 6.1 software with RGB system. D filter tetracycline marker images were tinted blue, N2.1 filter alizarin marker images were tinted red and I3 filter calcein marker images were tinted green. For the SEM-EDS analysis major elements that compose

the implant and bone were selected to be identified and quantified, the selected elements were titanium (Ti), calcium (Ca) and phosphorus (P) (Fig. 1). The mass percentage values of each element were counted at 400x magnification for comparison evaluation. From the same obtained SEM photos, image analysis was performed inside the implant, measuring implant area (Fig. 2A), bone area (Fig. 2B) and empty pore (Fig. 2C), all manually using ImagePro Plus 6.1 software.

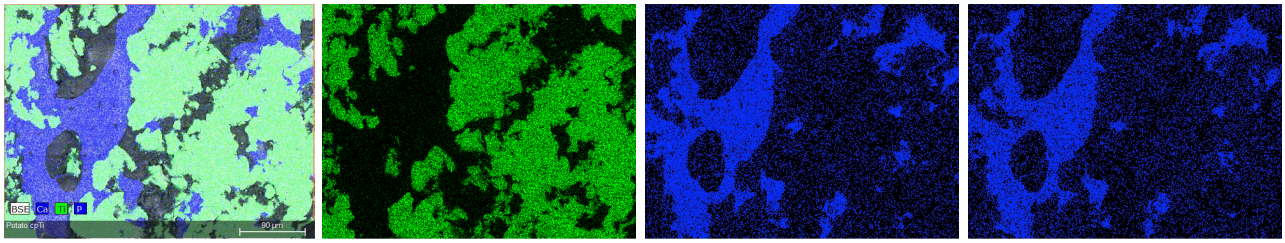

A B C D

Figure 1. Example of SEM-EDS analysis of cpTi sample: A) Composite image highlighting Ti, Ca, and P all together; B) Image highlighting only Ti, green color; C) Image highlighting only Ca, blue color; D) Image highlighting only P, blue color.

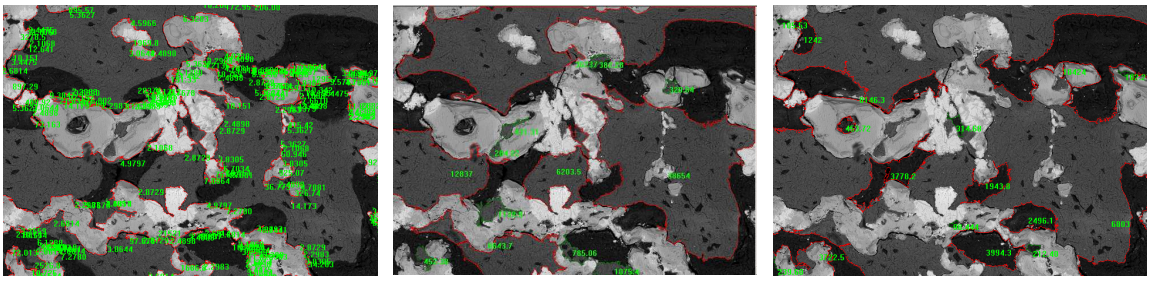

A B C

Figure 2. Example of image analysis of the bone-implant elements, delimited by red line: A) Implant area, represented by light grey, white color; B) Bone area, represented by dark grey color; C) Empty pores area, represented by black color.

Results and Discussion

As concluded in the previous publication [25], the TiH_2 powders proved to be a better raw material since it can withstand higher temperature during TT than metallic cpTi powder. The use of TiH_2 powder facilitates the processing of porous material, which can suffer oxidation during contact with the aqueous solution and during the TT step. As the mechanism of pore formation is the result of degradation of organic material by raising the temperature, it is necessary to perform the TT in an oxidizing atmosphere for complete removal of natural polymers added before sintering them at high vacuum.

In powder metallurgy (PM), morphology and size of the powder used is very important during the process, the shape of the particles will later influence the microarchitecture of the achieved pores. Through SEM the morphology of TiH_2 powder presented itself quite irregular (Fig. 3A). After sintering, the particles became rounded but maintained the precursor format, with necks formation between the particles (Fig. 3B). The roughness provides an increased surface area and the irregularities propitiate a friendly surface for cell attachment, as well as the improvement of the mechanical strength between bone and implant interface, a important clinical goal [7, 8].

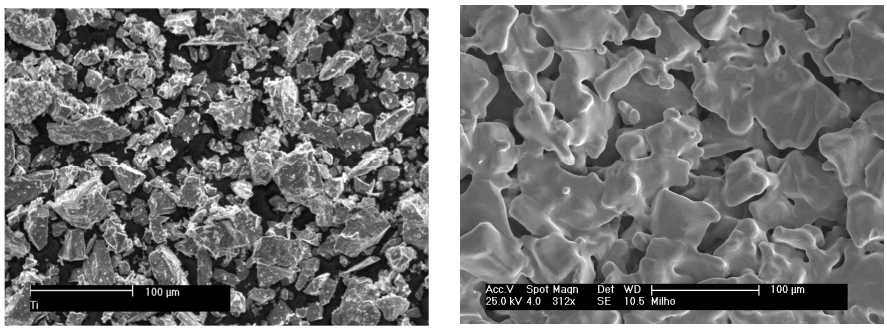

A B

Figure 3. SEM. A) TiH_2 powder morphology [25]. B) Example of surface morphology after sintering.

For comparison purpose with the metallic porous structures obtained in this study, SEM of rabbit proximal tibia trabecular bone was performed (Fig. 4). Different approach was observed, there is an overt highly porous structure, well distributed and with different pores size, some regions with heterogeneous pore size (Fig. 4A), another regions with homogeneous pore size (Fig. 4B), and other regions pores of irregular shape with non-defined format (Fig. 4C). It means that the trabecular bone have a very complex organization, ranging its own structure to meet the physical and metabolic need in response to physiological and environmental factors [4]. On a physic scale was possible to analyze the microarchitecture, porosity, lacunar morphology, pore size and distribution [27].

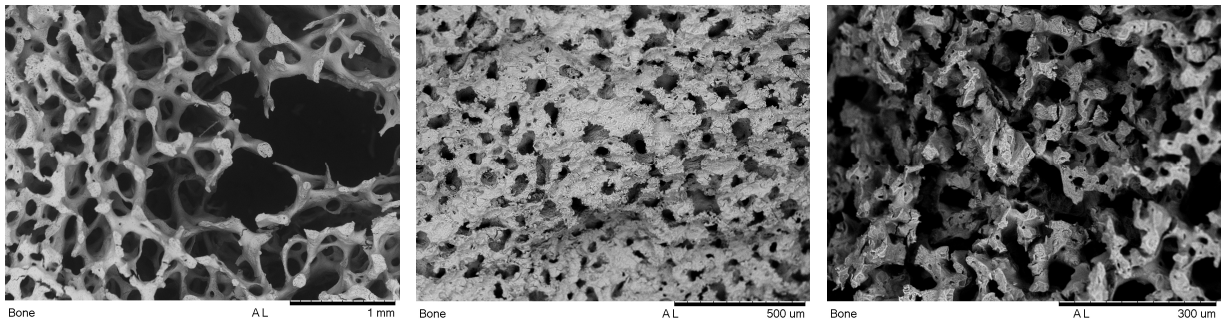

A B C

Figure 4. SEM of rabbit proximal tibia trabecular bone: A) Region with heterogeneous pore size distribution; B) Region with homogenous pore size distribution; C) Region with irregular pores shape.

The suspension technique described [25] using the different natural polymer additives, propitiated samples with no significant difference among porosity, the mean value was ~40%. But other aspects differentiate the samples obtained by those polymers, like the pore size and its distribution in the microstructure. According to the SEM analysis, all samples presented pores shape irregular with no standardized format. Although the additive used determined the pore size, pores were well distributed in the structure with no dense areas in the samples. The structure was achieved due to the linking of small titanium particles from the 3 dimensional dispositions of agglomerated polymer chains (following the each natural polymers), which resulted in an irregular lattice network structure.

The pore measurements were based on SEM and image analysis, the results were presented in Table 1. As control group, a dense and machined sample was used in the *in vivo* experiment, and also had its pores evaluated in order to compare with the porous groups. The small amount of pores in the dense structure had the mean diameter value of 21,4 µm, with a low standard deviation (0,2) meaning to be a very homogeneous pores. These pores are closed in the structure with no communication between them and outside (Fig.6).

Table 1. Values of pore size of the samples by image measurement analyze.

Samples	Pores size diameter (μm)			
	Max	Min	Mean	Std. Dev.
Dense	21,5	21,2	21,4	0,2
Corn	180,1	23,8	86,3	47,4
Potato	129,8	19,8	50,9	33,0
Rice	220,5	14,6	77,1	74,8
Gelatin	77,3	11,1	32,4	16,6

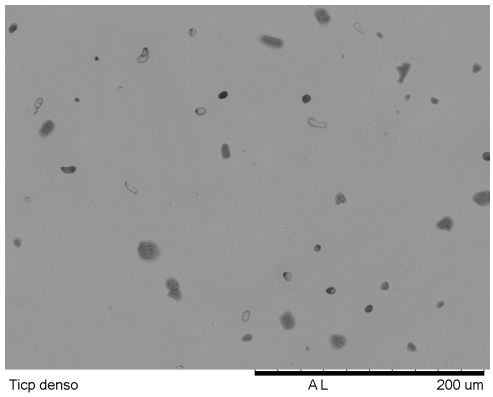

Figure 6. SEM of microstructure, dense sample (control group).

Samples added of cornstarch (Fig. 7, Table 1) the interconnectivity and the irregular shape of pores make difficult the measurement of a single pore, as a result of a high value of standard deviation. Similarly, addition of potato starch (Fig. 8, Table1) resulted in slightly smaller pores. The rice starch provided the most discrepant values of pore size, with the highest standard deviation (74,8) (Fig. 9, Table1). Compared to other groups, the rice starch promoted the most heterogeneous pores in the structure, differently to the gelatin added samples. The gelatin presented the lowest standard deviation indicating homogeneous pore size in the structure, (Fig. 10, Table1).

The samples added of rice starch (Fig. 9B) presented the most similar structure organization when compared to the bone tissue microstructure organization of the trabecular bone shown in Fig. 4C, which balances micropores and macropores distributed heterogeneously through the structure. The trabecular shape difference although similar design was the closest to mimic the microarchitecture of rabbit natural trabecular tibia bone in this study. Although the different natural polymers provided a similar aspect of porosity, the varying pore size and microstructure distribution, will determine the meets and needs to application of these porous metallic biomaterials based on each specific polymer, that holds the proper implant intrinsic features to achieve the repair and replacement success.

The bone microarchitecture is a well-discussed subject regarding the bone biomechanical characteristic. Besides, microarchitecture is one feature involved and directly determinant in the quality of bone, combined with hydroxyapatite crystal´s size, collagen type, quality and remodeling degree. The bone microarchitecture variation happens to mechanically adapt the bone to support loads which shifts direction, increase and decrease combined to a vary number of factors related to nutrition, metabolism, genetic, diseases, aging and the load itself [28].

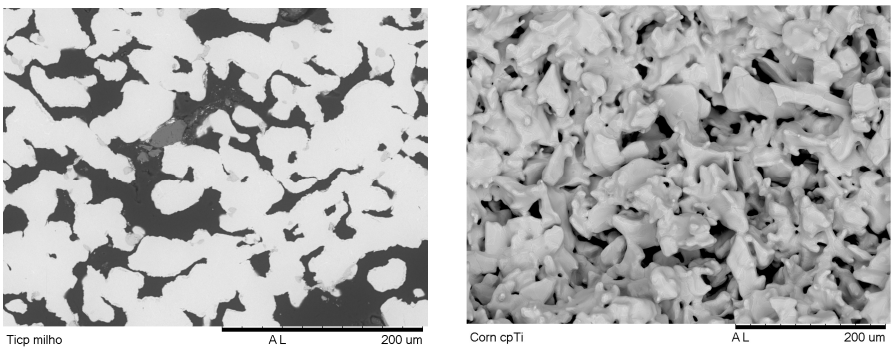

A B

Figure 7. SEM of microstructure of the samples added cornstarch: A) polished, B) fractured.

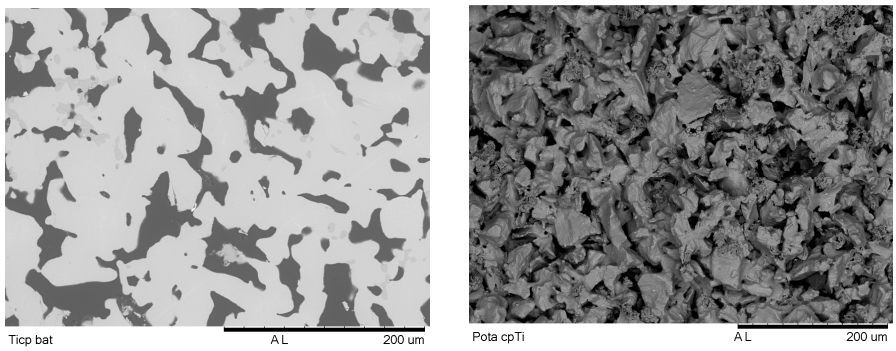

A B

Figure 8. SEM of microstructure of the samples added potato starch: A) polished, B) fractured.

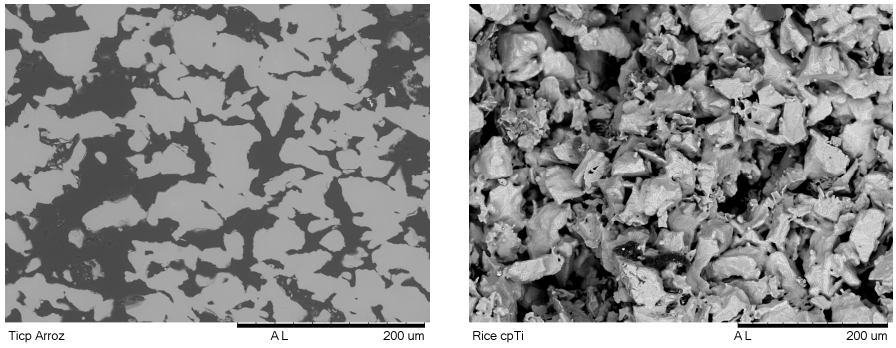

A B

Figure 9. SEM of microstructure of the samples added rice starch: A) polished, B) fractured.

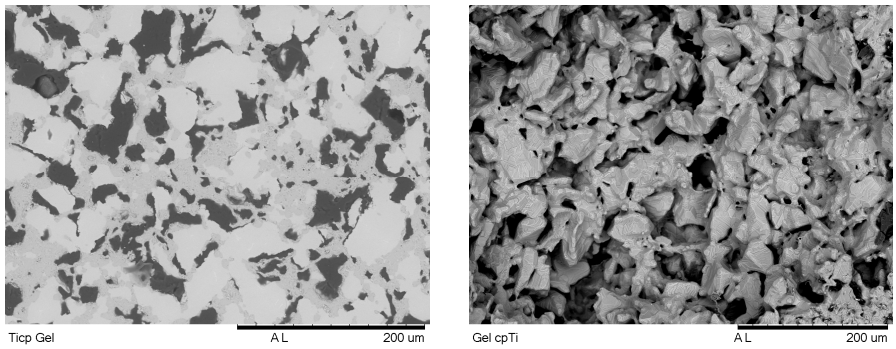

A B

Figure 10. SEM of microstructure of the samples added gelatin: A) polished, B) fractured.

For the histological evaluation, the undecalcified bone with implant, hard tissue processing technique, was used in order to provide the better condition to analyze the interaction between bone tissue and implant, their contact and interface on the implant's surface and inside its pores. A pattern was determined for all techniques from a control group (dense cpTi). The SEM of histological slices shows the osseointegration by a thin layer of mineralized bone tissue growth on the machined surface of the implant, characterizing the osteoconductive aspect of cpTi implants (Fig. 11A). By SEM-EDS a selected area inside the implant was analyzed, accounting for the ratio of elements: Ti, Ca and P (Fig. 11B). The cpTi implants recognized by Ti showed 99% of mass, the 1% value of Ca and P, refers to the displacement of particles during the polishing step on the histological slices. The SEM-EDS analyzes (Fig. 11C) showed the identification was standardized for areas of the implant (green area) and the bone (blue area) to compere with the porous groups. The FM analysis of control group (Fig. 11D), evaluates the bone remodeling process in the different phases of bone tissue repair and growth. Bone markers were applied systemically in rabbits, and by their affinity with calcium, they are deposited with apatite of the new bone [29]. With the analysis it

was possible to see the areas that represent the deposition of the marker during the growth bone, and relate them according to the emitted fluorescence with time and bone marker administered [19].

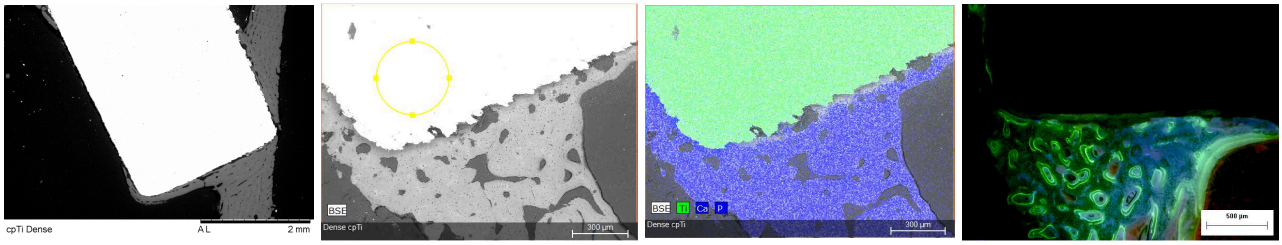

A B C D

Figure 11. Machined dense cpTi Implant: A) SEM of histological slide, osteoconduction through the surface of implant; B) SEM of histological slide showing in detail the interface bone-implant; C) SEM-EDS of histological slide of image presented on B; D) FM analysis of bone markers, bone-implant interface.

The importance of FM technique is showing the stages of bone growth and increase sensitivity in the assessment of bone growth inside pores, where, without the use of fluorescence, some areas could not be identified by conventional light microscopy. The enhancement of signal highlights those areas together with the correspondent cell growth stratification for each marker.

In the evaluation of metallic porous implants it was observed osseointegration, the mineralized bone tissue grew inside the pores with intimate contact through the material towards the center of the implant, characterizing the interconnect network of pores, able to sustain nourishing and proliferation of bone, enabled due to the known osteoconductivity of the titanium (Fig. 12: A, C, E). The identification of bone growth phases by FM analysis was performed through the evaluation of the fluorescent signaling from each fluorochrome marker in the bone tissue. With the obtaining of individual images for each fluorochrome marker in greysacle monochromatic besides reducing the noise inherent of colored images, the process of tinting the images with red, green, blue (RGB) color system and merging them, creates a tool that specifically separate the signal of each marker and highlights exactly the areas where they overlap each other, identifying the transition from one marker to another and as well where all markers are present. From the merging of RGB color system tinted images areas of superposition of markers were presented by the combination of their primary colors, hence the yellow provided by the combination of red with green colored images, the magenta from the combination of red with blue colored images, cyan from the combination of blue with green colored images and white from the combination of all three colors.

The tetracycline images tinted with blue color in the FM analysis, also represented as magenta in combination with red color (Alizarin) and cyan color in combination with green (Calcein), had a good expressiveness on all implants, especially the ones with smaller pores. This can be explained by the fact that the first wave of progenitor bone cells and bone growth can permeate through all size of pores initially, but the sustaining of bone growth depends on pores which provide enough space for nourishing, evidencing that for this first bone cell spreading the size of the pore plays a lower role, while the major role still belongs to the material intrinsic features. Although the amount of progenitor cells and repair tissue present at the first stage of tissue response to the implant are responsible for the faster bone maturation, perpetuation of the bone growth and remodeling (Fig. 12H). The alizarin images tinted with red color in the FM analysis, also represented as magenta in combination with blue color (Tetracycline) and yellow in combination with green color (Calcein), presented the least expressive marker from the three used in this study, although present in all samples and dispersed diffusely in areas of superposition of markers through the tissue, showing that the maturing and deposition of bone matrix is a ongoing process which involves deposition, organizing and remodeling over time (Fig. 12D). The calcein images tinted with green color in the FM analysis, also represented as yellow in combination with red color (Alizarin) and represented as cyan in combination with blue color (Tetracycline), had the higher expressiveness on implants. This means that the maturing and growth of bone, as well the deposition of mineralized bone matrix was

carried out through all the experiment period, especially on the final third of it. Although more evident on implants with bigger pores that allowed a deeper bone penetration towards the center of implants, it showed that these porous metallic implants induced a continuous bone deposition during the studied period (Fig. 12: A, B, C, D, E, F). To elucidate better until when this process would be maintained and stimulated by the implant features, longer periods experiments are needed. In all images the observation of white color represented by the combination of blue (Tetracycline), red (Alizarin) and green (Calcein) colors indicates the presence of all three markers in that area, showing and corroborating with the ongoing process of bone maturing, depositing and remodeling during all the experiment period. Table 2 shows the result of semi-quantitative evaluation of the fluorescent signal with the respective signal intensity score based on 1+ (weak), 2+ (moderate) and 3+ (strong) for each fluorochrome evaluated within the implant after obtaining the final image.

Based on these results, it is possible to assert that all pores size allowed the first stage of bone ingrowth, the penetrance of progenitor bone cells. But homogeneous and small pores (bellow 80 µm) can limit the maturing process of bone towards the center of implant, for not provide enough space for nourishing. On the other hand, pores bigger than that allowed faster bone maturation, perpetuation of the bone growth and remodeling, besides bone penetration towards the center of implants.

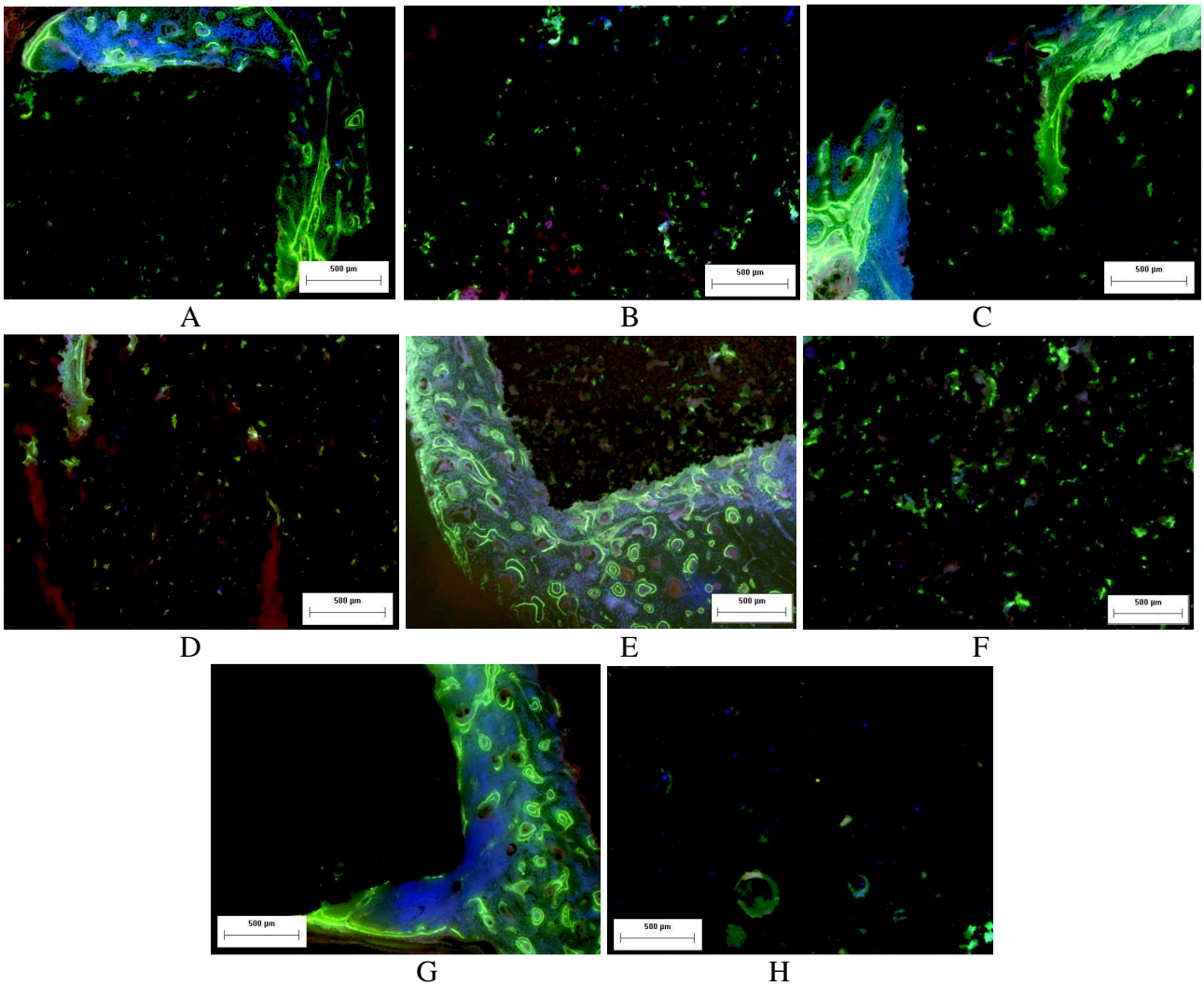

Figure 12. Bone ingrowth of samples added: cornstarch (A, B), potato starch (C, D), rice starch (E, F) and gelatin (G, H). A, C, E, G) Fluorescent microscopy of bone markers, bone-implant interface; B, D, F, H) Fluorescent microscopy of bone markers, interior implant area.

Table 2. Semi-quantitative analyses of the fluorescent bone markers intensity inside the implants.

Implant	Fluorescent markers		
	Tetracycline	Alizarin	Calcein
Dense*	2+	1+	3+
Corn	1+	1+	3+
Potato	1+	3+	3+
Rice	2+	2+	3+
Gelatin	2+	1+	2+

* Surrounding area.

Table 3. Quantitative analyses of formed new bone and implant area, by SEM-EDS and Image analysis.

Implant	EDS		Image analysis		
	cpTi	Ca/P	Bone	Porous	Implant
Dense	99%	1%	-	-	-
Corn	96%	5%	8%	6%	86%
Potato	96%	4%	24%	19%	57%
Rice	93%	7%	12%	20%	68%
Gelatin	93%	7%	10%	20%	70%

The evaluation by SEM and SEM-EDS analysis of histological slides allows quantifying and qualifying the bone tissue inside the pores, besides presenting higher sensitivity in identifying the bone in side the porous implant, when compared with the FM analysis. By SEM-EDS analysis all bone growing inside pores is highlighted, which is an important factor to use this technique when evaluating metallic porous implants. With FM analysis it is possible to identify the bone growth phases and filling areas related to the post implantation period. On Fig. 13, it is possible to observe linked micropores filled with bone tissue, which can be verified by the presence of osteocytes lacunae imprisoned on the mineral matrix. The quantifying of bone, pore and implant, was performed with image analysis protocol cited before for each sample, and the results are presented on Table 3. The SEM-EDS analysis despite being a semi-quantitative method, allowed the differencing the metallic, pore and bone areas. Evidenced by the elements present in both materials exclusively, depicting a map corresponding to each material.

It is common when studying implants on bone to use conventional histological staining methods to assess the bone response. Although very well established for decalcified bone tissue slides, those staining methods, protocols and procedures when applied to undecalcified bone tissue with metallic implants must be adapted and validated. Results are not on the same level as of its decalcified counterpart, while considering the morphological aspects of bone, this is even more evidenced with porous metallic implants in which bone tissue grew inside of the material. The fact that no matter how thin the histological become metal will not be translucent, therefore there will always be areas of bone-implant interface that will not be evaluated properly. Thus the use of a different approach on the assessment of bone-implants combining SEM, SEM-EDS and FM analysis present a much more reproductive process and reliable evaluation with higher sensitivity in detecting bone inside pores, as well as bone-implant interface, which is the main goal evaluating porous metallic biomaterials.

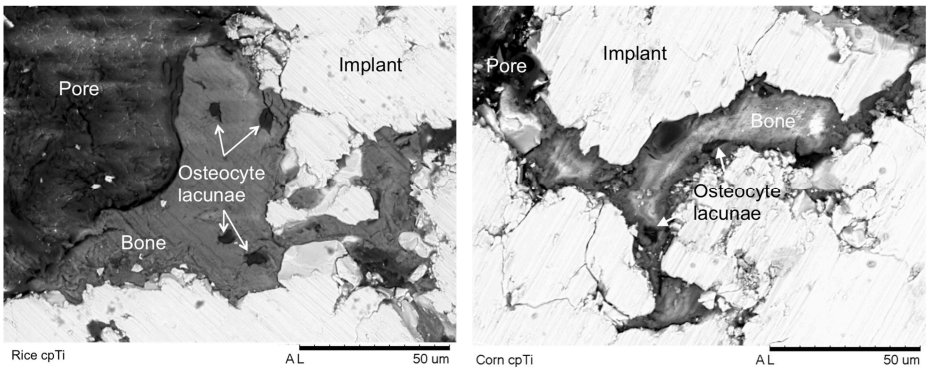

A B

Figure 13. SEM of undecalcified histological slide presenting bone-implant interface and pores; osteocyte lacunae indicated by arrows: A) Implant obtained with rice starch, B) Implant obtained with cornstarch.

By the SEM and SEM-EDS analysis the regions referent to the bone and to the implant were standardized (Fig. 14 A, B, C, D). The porous cpTi implants identified on the SEM-EDS analysis by the element Ti presented 90 to 96% in mass, while bone identified by elements Ca and P presented 4 to 7% in mass. The discrepant result when comparing the percentage value for each component and the area of each on the image can be explained by the fact that this measurement is performed counting the percentage in mass of the elements, while titanium implants are assumed to have only Ti in its composition, bone on the other hand is composed by proteins, glycoproteins, sugars, hydroxyapatite, DNA, RNA so on and so forth, when identifying Ca and P on bone tissue it is aiming for two elements present on the mineralized matrix majorly composed by hydroxyapatite ($Ca_{10}(PO_4)_6(OH)_2$). For this reason the values were not used to inference, but only for comparison between the experimental groups, albeit the elements identification together with their mapping where used to prove the bone presence and growth inside implant pores. The quantifying on SEM images of the percentage in area of implant, bone and pore were performed by image analysis and the results are presented together on Table 3. Based on the image analysis were observed that for the correspondent area of pores, half to two thirds of its total area were filled with mineralized bone matrix. The filling of pores by bone proved their interconnectivity, also that the size of the pores were suitable for bone ingrowth, although their measurement is difficult due to its irregular 3 dimensional shape forming a highly interconnected network of channels.

The tools used to the histological evaluation of this study, allowed a simplified identification of new bone tissue. By SEM, was possible to observe the bone-implant interaction, and the cellular characterization was evaluated by morphology. The SEM-EDS analysis was able to qualify and quantify the major constituents elements of implant and bone, in this case Ti, Ca and P, respectively. The FM analysis evaluating fluorescent bone markers complemented the results, showing the phases of bone tissue growing and remodeling inside implants' pores.

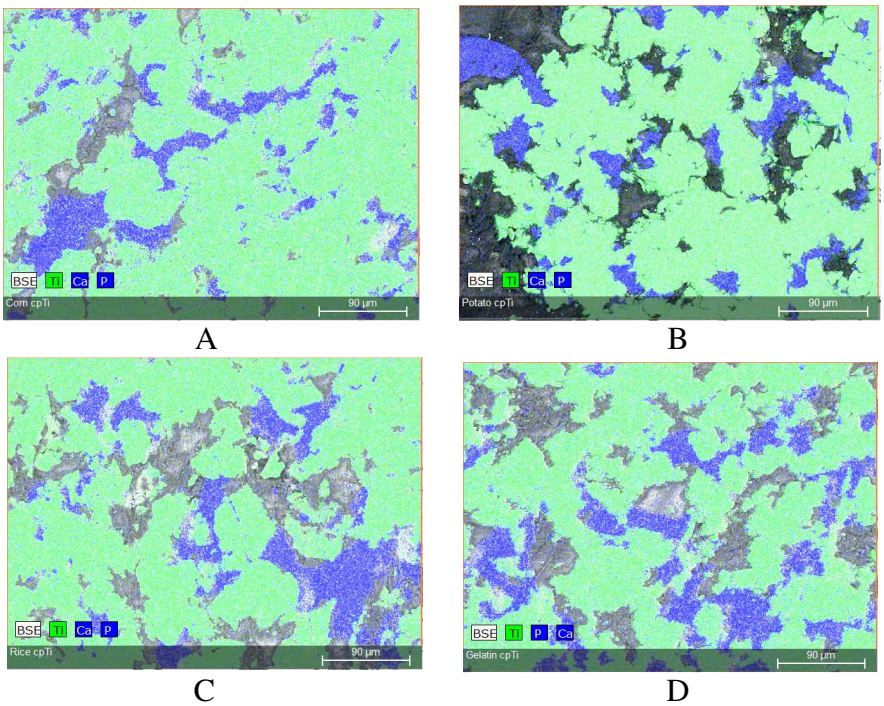

Figure 14. SEM-EDS of histological slice, showing pores (grey), bone (blue) and implant (green) areas, of samples added: A) cornstarch, B) potato starch, C), rice starch, D) gelatin.

Conclusions

The mimicking of trabecular bone architecture was achieved by the PM technique with addition of natural polymer as pore formation agent used in this study. Especially the rice starch, that presented the most similar structure organization when compared to the bone tissue microstructure

organization of the trabecular bone, which balances micropores and macropores distributed heterogeneously through the structure.

Although the osseointegration had occurred in all implants, by the bone ingrowth in the pore microarchitecture and its interconnected network, the pore size determined the speed of bone maturation and penetration towards the center of implants. Pores smaller than 80μm, allowed some bone maturation with little penetration inside the implant core, while pores bigger than that allowed continuous bone maturation with high penetration inside the implant.

The tools used to the histological evaluation of this study, allowed a simplified identification of new bone tissue. The evaluation by SEM-EDS analysis was successful to detect bone inside the pores of implant, as well as to identify the elements that constitute the implant and bone, on histological slices of undecalcified bone tissue implant. The evaluation by FM analysis distinguished the bone growth phases through time inside implants, based on fluorescent bone markers.

Acknowledgements

The authors are grateful to the Brazilian institutions, FAPESP and CNPq for financial support.

References

[1] R.L. Oréfice, M.M. Pereira, H.S. Mansur, Biomateriais – Fundamentos e Aplicações, first ed., Ed. Cultura Médica, Rio de Janeiro, 2006.

[2] D.A. Puelo, A. Nanci, Undestanding and controlling the bone-implant interface, Biomaterials. 20 (1999) 2311-2321.

[3] J.E. Lemons, Biomaterials, biomechanics, tissue healing, and immediate-function dental implants, J. Oral Implantol. 30 (2004) 318-324.

[4] R.Z. Legeros, R.G. Craig, Strategies to affect bone remodeling: osteointegration. J. Bone Miner. Res. 8 (1993) 583-596.

[5] M. Weinlaender, Bone growth around dental implants, Dent. Clin. North. Am. 35 (1991) 585-601.

[6] L.C. Junqueira, J. Carneiro, Histologia básica, eighth ed., Guanabara Koogan, Rio de Janeiro, 1995.

[7] X. Liu, P.K. Chu, C. Ding, Surface modification of titanium, titanium alloys, and related materials for biomedical applications, Mat. Science Eng. R. 47 (2004) 49-121.

[8] S. Franz, S. Rammelt, D. Scharnweber, J.C. Simon, Immune responses to implants - A review of the implications for the design of immunomodulatory biomaterials, Biomat. 32 (2011) 1-18.

[9] H. Shen, L.C. Brinson, Anumerical invention of porous titanium as orthopedic implant material. Mech. Mat. 8 (2011) 420-430.

[10] A.I. Itäla, H.O. Ylanen, C. Ekholm, K.H. Karlsson, H.T. Aro, Pore diameter of more than 100 micron is not requisite for bone ingrowth in rabbits. J. Biomed. Mater. Res. 58 (2001) 679-683.

[11] S. Kujala, J. Ryhänen, A. Danilov, J. Tuukkanen, Effect of porosity on the osteointegration and bone ingrowth of a weight-bearing nickel–titanium bone graft substitute, Biomat. 24 (2003) 4691-4697.

[12] G. Ryan, A. Pandit, D.P. Apatsidis, Fabrication methods of porous metals for use in orthopaedic applications, Biomat. 27 (2006) 2651-2670.

[13] A. Laptev, M. Bram, H.P. Buchkkemer, D. Stover, Study of production route for titanium parts combining very high porosity and complex shape, Powder Metal. 47 (2004) 85-92.

[14] J. Li, H. Liao, B. Fartash, L. Hermansson, T. Johnsson, Surface-dimpled commercially pure titanium implant and bone ingrowth, Biomat. 18 (1997) 691-696.

[15] M. Takemoto, S. Fujibayashi, M.Neo, J. Suzuki, T. Kokubo, T. Nakamura, Mechanical properties and osteoconductivity of porous bioactive titanium, Biomat. 26 (2005) 6014-6023.

[16] H.E. Götz, M. Müller, A. Emmel, U. Holzwarth, R.G. Erben, R. Stangl, Effect of surface finish on the osseointegration of laser-treated titanium alloy implants, Biomat. 25 (2004) 4057–4064.

[17] S.C.P. Cachinho, R.N. Correia, Titanium scaffolds for osteointegration: mechanical, in vitro and corrosion behavior, J. Mater. Sci: Mater. Med. 19 (2008) 451–457.

[18] A.E. Aguikar Maya, D.R. Grana, A. Hazarabedian, G.A. Kokubo, M.I. Luppo, G. Vigna, Zr-Ti-Nb porous alloy for biomedical application, Mat. Science Eng. C. 32 (2011) 321-329.

[19] T.S. Goia, K.B. Violin, M. Yoshimoto, J.C. Bressiani, A.H.A. Bressiani, Osseointegration of Titanium Alloy Macroporous Implants Obtained by PM with Addition of Gelatin, Adv. Science Techn. 76 (2010) 259-263.

[20] O.M. Ferri, T. Ebel, R. Bormann, Influence of surface quality and porosity on fatigue behaviour of Ti–6Al–4V components processed by MIM, Mat. Science Eng. A. 527 (2010) 1800–1805.

[21] J.C. Li, D.C Dunand, Mechanical properties of directionally freeze-cast titanium foams. Acta Mat. 59 (2011) 146-158.

[22] P. Heinl, L. Müller, C. Körner, R.F. Singer, F.A. Müller, Cellular Ti–6Al–4V structures with interconnected macro porosity for bone implants fabricated by selective electron beam melting. Acta Biomat. 4 (2008) 1536–1544.

[23] F.E. Wiria, J.Y.M. Shyan, P.N. Lim, F.G.C. Wen, J.F. Yeo, T. Cao, Printing of Titanium implant prototype. Mat. Design. 31 (2010) S101–S105.

[24] E. Gregorová, W. Pabst, I. Bohačenko, Characterization of different starch types for their application in ceramic processing, J. Eur. Ceram. Soc. 26 (2006) 1301-1309.

[25] T.S. Goia, K.B. Violin, J.C. Bressiani, A.H.A. Bressiani, Mimicking Bone Architecture in a Metallic Structure, Adv. Science Techn. 84 (2013) 7-12.

[26] E. Gemelli, N.H.A. Camargo, Oxidation kinetics of commercially pure titanium, Rev. Matéria. 12 (2007) 525-531.

[27] C.J. Hernandez , T.M. Keaveny, A biomechanical perspective on bone quality, Bone. 39 (2006) 1173–1181.

[28] D. Chappard, M.-F. Baslé, E. Legrand, M. Audran, Trabecular bone microarchitecture: A review, Morphologie. 92 (2008) 162—170.

[29] C. Pautke, S. Vogt, K. Kreutzer, C. Haczek, G. Wexel, A. Kolk, A.B. Imhoff, H. Zitzelsberger,5 S. Milz, T. Tischer, Characterization of eight different tetracyclines: advances in fluorescence bone labeling, J. Anat. 217 (2010) 76-82.

Journal of Biomimetics, Biomaterials and Biomedical Engineering Vol. 20
10.4028/www.scientific.net/JBBBE.20

Bone Tissue Response in a Metallic Bone Architecture Microstructure
10.4028/www.scientific.net/JBBBE.20.73

DOI References
[2] D.A. Puelo, A. Nanci, Undestanding and controlling the bone-implant interface, Biomaterials. 20 (1999) 2311-2321.
http://dx.doi.org/10.1016/S0142-9612(99)00160-X
[3] J.E. Lemons, Biomaterials, biomechanics, tissue healing, and immediate-function dental implants, J. Oral Implantol. 30 (2004) 318-324.
http://dx.doi.org/10.1563/0712.1
[4] R.Z. Legeros, R.G. Craig, Strategies to affect bone remodeling: osteointegration. J. Bone Miner. Res. 8 (1993) 583-596.
http://dx.doi.org/10.1002/jbmr.5650081328
[7] X. Liu, P.K. Chu, C. Ding, Surface modification of titanium, titanium alloys, and related materials for biomedical applications, Mat. Science Eng. R. 47 (2004) 49-121.
http://dx.doi.org/10.1016/j.mser.2004.11.001
[8] S. Franz, S. Rammelt, D. Scharnweber, J.C. Simon, Immune responses to implants - A review of the implications for the design of immunomodulatory biomaterials, Biomat. 32 (2011) 1-18.
http://dx.doi.org/10.1016/j.biomaterials.2011.05.078
[11] S. Kujala, J. Ryhänen, A. Danilov, J. Tuukkanen, Effect of porosity on the osteointegration and bone ingrowth of a weight-bearing nickel-titanium bone graft substitute, Biomat. 24 (2003) 4691-4697.
http://dx.doi.org/10.1016/S0142-9612(03)00359-4
[12] G. Ryan, A. Pandit, D.P. Apatsidis, Fabrication methods of porous metals for use in orthopaedic applications, Biomat. 27 (2006) 2651-2670.
http://dx.doi.org/10.1016/j.biomaterials.2005.12.002
[13] A. Laptev, M. Bram, H.P. Buchkkemer, D. Stover, Study of production route for titanium parts combining very high porosity and complex shape, Powder Metal. 47 (2004) 85-92.
http://dx.doi.org/10.1179/003258904225015536
[14] J. Li, H. Liao, B. Fartash, L. Hermansson, T. Johnsson, Surface-dimpled commercially pure titanium implant and bone ingrowth, Biomat. 18 (1997) 691-696.
http://dx.doi.org/10.1016/S0142-9612(96)00185-8
[15] M. Takemoto, S. Fujibayashi, M. Neo, J. Suzuki, T. Kokubo, T. Nakamura, Mechanical properties and osteoconductivity of porous bioactive titanium, Biomat. 26 (2005) 6014-6023.
http://dx.doi.org/10.1016/j.biomaterials.2005.03.019
[16] H.E. Götz, M. Müller, A. Emmel, U. Holzwarth, R.G. Erben, R. Stangl, Effect of surface finish on the osseointegration of laser-treated titanium alloy implants, Biomat. 25 (2004) 4057-4064.
http://dx.doi.org/10.1016/j.biomaterials.2003.11.002
[18] A.E. Aguikar Maya, D.R. Grana, A. Hazarabedian, G.A. Kokubo, M.I. Luppo, G. Vigna, ZrTi-Nb porous alloy for biomedical application, Mat. Science Eng. C. 32 (2011) 321-329.
http://dx.doi.org/10.1016/j.msec.2011.10.035

[19] T.S. Goia, K.B. Violin, M. Yoshimoto, J.C. Bressiani, A.H.A. Bressiani, Osseointegration of Titanium Alloy Macroporous Implants Obtained by PM with Addition of Gelatin, Adv. Science Techn. 76 (2010) 259-263.
http://dx.doi.org/10.4028/www.scientific.net/AST.76.259
[20] O.M. Ferri, T. Ebel, R. Bormann, Influence of surface quality and porosity on fatigue behaviour of Ti-6Al-4V components processed by MIM, Mat. Science Eng. A. 527 (2010) 1800- 1805.
http://dx.doi.org/10.1016/j.msea.2009.11.007
[24] E. Gregorová, W. Pabst, I. Bohačenko, Characterization of different starch types for their application in ceramic processing, J. Eur. Ceram. Soc. 26 (2006) 1301-1309.
http://dx.doi.org/10.1016/j.jeurceramsoc.2005.02.015
[25] T.S. Goia, K.B. Violin, J.C. Bressiani, A.H.A. Bressiani, Mimicking Bone Architecture in a Metallic Structure, Adv. Science Techn. 84 (2013) 7-12.
http://dx.doi.org/10.4028/www.scientific.net/AST.84.7
[27] C.J. Hernandez , T.M. Keaveny, A biomechanical perspective on bone quality, Bone. 39 (2006) 1173-1181.
http://dx.doi.org/10.1016/j.bone.2006.06.001
[28] D. Chappard, M. -F. Baslé, E. Legrand, M. Audran, Trabecular bone microarchitecture: A review, Morphologie. 92 (2008) 162-170.
http://dx.doi.org/10.1016/j.morpho.2008.10.003